Influence of gas environment on the dynamics of wetting transition of laser-textured stainless steel meshes

V. V. Kim, V. S. Yalishev, S. A. Khan, et al.

View Online　　**Export Citation**　　**CrossMark**

ARTICLES YOU MAY BE INTERESTED IN

Carbon nanostructure containing plasma: Medium for efficient high-order harmonics of 1030 nm laser
Physics of Plasmas **28**, 023111 (2021); https://doi.org/10.1063/5.0035758

Thermodynamic analysis and prediction on the wetting properties of pore array superhydrophobic laser-texturing surfaces
Journal of Applied Physics **129**, 215302 (2021); https://doi.org/10.1063/5.0050644

Femtosecond laser-induced periodic surface structures
Journal of Laser Applications **24**, 042006 (2012); https://doi.org/10.2351/1.4712658

READ NOW!

AIP Advances
Photonics and Optics Collection

Influence of gas environment on the dynamics of wetting transition of laser-textured stainless steel meshes

View Online   Export Citation   CrossMark

V. V. Kim,[1] (ID) V. S. Yalishev,[1] (ID) S. A. Khan,[1] M. Iqbal,[1] (ID) G. S. Boltaev,[1] (ID) R. A. Ganeev,[1,2,a)] (ID)
and A. S. Alnaser[1,b)] (ID)

AFFILIATIONS

[1] Department of Physics, American University of Sharjah, Sharjah 26666, United Arab Emirates
[2] Institute of Astronomy, University of Latvia, Riga LV-1586, Latvia

a)Author to whom correspondence should be addressed: rashid_ganeev@mail.ru
b)aalnaser@aus.edu

ABSTRACT

We analyze the role of surrounding gas and aging in ambient air in the wettability behavior of laser-processed stainless steel meshes. Laser texturing of meshes was carried out in the presence of different gases (N_2, O_2, CO_2, Ar, and SF_6) in ambient atmospheric air and under different vacuum conditions. The influence of each gas on the evolution of the wettability properties after aging in ambient air is analyzed. The effects of low-pressure and vacuum aging allowed transforming the initial superhydrophilic characteristics of the laser-structured meshes to an almost superhydrophobic state.

I. INTRODUCTION

The wettability of a material's surface is an important property that plays a crucial role in a wide range of surface-related phenomena and defines different ranges of applications. In the case of stainless steel, the industrial applications are countless and can be enhanced by controlling its surface properties. The surface properties of steel, such as color, chemical stability, roughness, and wettability, have received special attention in biomedicine, optics, and surface chemistry.[1–4] Wetting is the ability of a liquid medium to maintain contact with a solid medium due to intermolecular interaction while in contact with each other. Static contact angle θ is a quantitative way to measure the wettability at the solid–liquid interface.[5] Different strategies have been proposed to tune the wetting behavior of metal surfaces. Most of them require the use of coatings with suitable materials or plasma/chemical etching. Recently, controlling the extreme wetting properties of materials by laser texturing of the surface of the substrate has gained much attention because it is a maskless, chemical free, facile, and robust technique.[6]

Laser texturing of metal surfaces is proven to be a reliable way to change the wettability of materials, with transitions toward superhydrophilic or superhydrophobic properties depending on the material surface energy. For low surface energy materials, such as polytetrafluoroethylene (Teflon), laser structuring can enhance the superhydrophobic characteristic,[7] whereas for other freshly laser textured materials, it yields a superhydrophilic response.[8,9] Laser processing of metals in ambient air by femtosecond laser pulses produces metal oxides on the textured surfaces. Metal oxides possess high surface energy and typically behave as hydrophilic materials because oxides favor the formation of hydroxylated layers through hydrogen bonding.[10] Laser texturing leads to the formation of various micro- and nanostructures on the surface of the material. The shape and content of these structures can be controlled by laser parameters, such as pulse energy, polarization, and scanning speeds. Generally, laser surface structuring is accompanied by the functionalization step to alter or retain the desirable surface wettability of materials. Meanwhile, the wettability of laser-textured metal surfaces can be changed from hydrophilic to hydrophobic if the textured surface is exposed to air for an extended period of time. Such transitions

were observed for stainless steel,[9,11] aluminum alloys,[8,12] and other metal alloys.[13,14]

Generally, surfaces immediately after laser treatment are hydrophilic ($\theta_w < 30°$, where θ_w is the static contact angle in the case of water). Within one week of exposure to air, the wettability changes to hydrophobic ($\theta_w \approx 90°$), and within two weeks or more, the surfaces become superhydrophobic with $\theta_w \approx 150°$. The exposure to air does not change the morphology of the micro/nanostructures. However, the surface is influenced by chemical changes. Different processing environments, including O_2, air, N_2, CO_2, and Ar, during laser texturing of stainless steel and aluminum were studied in Refs. 15 and 16. These studies have shown that laser processing and aging in different environments influence the wettability transition rate.

Stainless steel in the form of meshes is a robust, durable, and flexible construction material. Recently, controlling the wettability state of metal meshes by femtosecond laser-induced structuring has found applications in efficient oil–water separation.[17,18] In this work, the role of the processing atmosphere, as well as the influence of the long term aging in ambient air of the laser-processed stainless steel meshes on their wettability, is studied. The role of low pressure and vacuum storing is also tested. Our studies show that low pressure and vacuum aging allow transforming the initial superhydrophilic characteristics of laser-structured meshes to an almost superhydrophobic state.

II. MATERIALS AND METHODS

The stainless steel meshes were processed by laser radiation in the presence of five gases (N_2, O_2, CO_2, Ar, and SF_6) as well as in ambient atmospheric air and vacuum conditions. We used a femtosecond laser source (FS) at a central wavelength of 1030 nm. After processing, the laser-textured meshes were aged in the ambient air conditions for 30 days under the same conditions while maintaining constant temperature and humidity. To analyze the effect of vacuum aging on the wetting characteristic, two different chambers were used. One of them utilized an oil-free vacuum pump system, while the second chamber used the pump system containing oil as a lubricant for the moving parts.

Figure 1 shows the experimental setup used for the laser treatment of the meshes in various gas atmospheres. The femtosecond laser beam (FS) from a high-power fiber-based laser system (AFS-UFFL-300-2000-1030-300, Active Fiber Systems GmbH) with a central wavelength of 1030 nm, a repetition rate of 50 kHz, an average power of 5 W, and a pulse duration of 40 fs was used for laser structuring of meshes. Laser radiation was focused and raster scanned on the sample by the 160 mm F-Theta lens and scanning head (SH) (FARO tech. Xtreme-20) as shown in Fig. 1. The scanning head was mounted outside the vacuum chamber, and the scanning beam was directed inside the chamber through a quartz window. The laser surface texturing of stainless steel meshes was carried out using a similar geometry by the bi-directional line-by-line scanning strategy. The distance between scan lines was set to 60 μm. The focused laser beam spot diameter was measured to be ~100 μm. The single pulse energy was equal to 100 μJ.

Meshes with a size of 2 × 2 cm^2 were processed by laser radiation inside the enclosed chamber in the presence of different gases, in atmospheric air, or at the vacuum conditions. Gases (N_2, O_2, CO_2,
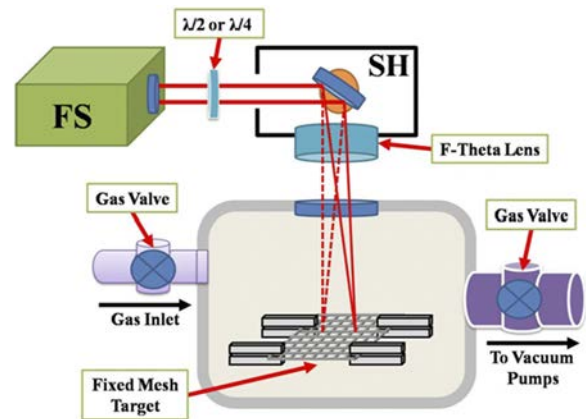

FIG. 1. Experimental setup. The beam from the femtosecond laser source (FS) was controlled by the scanning head (SH) and focused inside the vacuum chamber on the surface of the mesh target. The polarization properties of laser radiation were controlled using $\lambda/2$ or $\lambda/4$ waveplates. Two gas valves were used to control gas pressure inside the chamber or to maintain vacuum conditions. The mesh target inside the chamber was fixed in a way that no material existed behind mesh pores and no deposition from any other material occurred.

Ar, and SF_6) with 99.95% purity were used. The meshes inside the chamber were fixed in a way that no material behind mesh pores existed and no deposition from any other material occurred. The scanning speed was varied from 50 to 300 mm/s. With the estimation of the focusing spot area, the laser fluence on the target area was 1.2 J/cm^2. In the case of ablation in atmospheric air, the ablation threshold was estimated to be around 0.07 J/cm^2. The number of overlapped pulses was varied from 16 to 100 depending on the scanning speed. The polarization direction of the laser beam was controlled by the $\lambda/2$ waveplate. The circular polarization (CP) was maintained by using the $\lambda/4$ waveplate. Different vacuum pump systems were used in our experiments with two chambers, which we designate as Chamber No. 1 and Chamber No. 2. In Chamber No. 1, we used the pair of "oil-less" pumps (Edwards nXDS 6i and Pfeiffer HiPace 30 turbopump). Chamber No. 2 utilized another pair of pumps, one of which (Pfeiffer DUO 2.5) used the vacuum oil (Edwards Ultragrade 19) as a lubricant. In both chambers, a vacuum pressure of 2×10^{-4} mbar was maintained during these experiments. The gas pressure was controlled by two gas valves. The first valve was placed before the vacuum pump system, and the second one controlled the gas inlet.

Following laser treatment, the surface morphology of the surface was analyzed using a scanning electron microscope (SEM) (TESCAN VEGA3), and the surface chemistry was evaluated via energy-dispersive x-ray spectroscopy (EDS) using the SEM x-ray detector. For wettability characterization, the water contact angle (WCA) was measured using a Drop Shape Analyzer (KRUSS). Distilled water droplets (~5 μl volume) were used for all samples to determine the WCA.

Stainless steel meshes (316 L) with a pore size of 150 μm and a mesh wire thickness of 100 μm were used because of their high mechanical strength, durability, and commercial availability. Meshes were purchased from Sigma-Aldrich. Figure 2 shows the SEM images of the untreated mesh. Note that the surface of wires
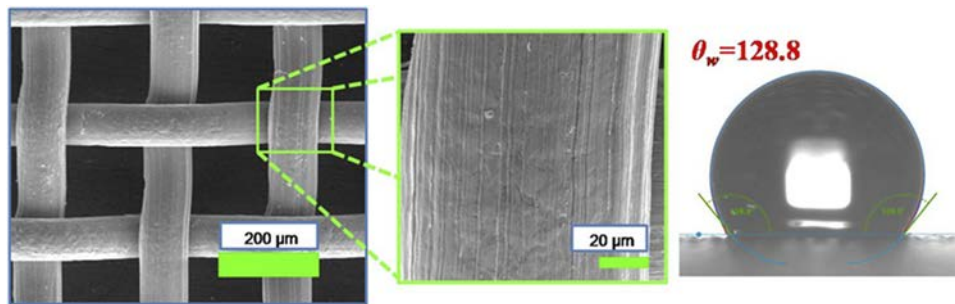
FIG. 2. SEM images of the untreated stainless steel mesh and measured water contact angle.

had structures in the form of lines along the wire direction, and some irregularities at the positions of wires overlap, which result from the manufacturing method of the wires and meshes. These structures with a combination of mesh geometry could be responsible for the relatively high WCA for untreated meshes (~128°). After preparation, the laser textured meshes were aged in ambient air for 30 days under the same conditions and at constant temperature and humidity (21.5 °C and 45% humidity).

III. RESULTS AND DISCUSSION

A. Surface morphology

First, we describe the process of sample preparation using different gases. Mesh samples were structured inside Chamber No. 1. An air pressure of 1 atm was purged inside the chamber for the laser treatment of meshes at ambient conditions. In the case of different gases, the procedure was as follows: Initially, we pumped the chamber with meshes inside down to the vacuum condition of 2×10^{-4} mbar. Then, the sample was stored at these conditions for 30 min, allowing additional cleaning and gas removal from the surface of the sample. Then, in the case of treatment in a particular gas environment, the valve between the chamber and pump line was closed and the gas was introduced into the chamber. For all gases, the same pressure of about 200 mbar was used. After gas purging,

the sample was textured by laser radiation. Finally, before opening the chamber, the treated sample was stored for 2 h in the same gas environment. Immediately after extracting from the chamber, the sample was tested to measure the WCA. In the case of laser treatment in atmospheric air or only in vacuum, the same storing time was used. Alongside with the influence of the gas environment, the variation of scanning speed and polarization laser radiation caused the morphology and wettability variations.

The morphology of the laser-textured surfaces prepared in ambient air is shown in Fig. 3. The direction of laser scanning is shown by blue arrows, and the polarization direction is shown by white arrows and a white circle. Changing the scanning speed with the same single pulse fluence led to the formation of the periodic submicrometer- and micrometer-sized ripples at a low number of overlapped beams (Fig. 3, bottom; scanning speed: 300 mm/s) and microgrooves at a larger number of overlapped beams (Fig. 3, top; scanning velocity: 50 mm/s). This method can form the quasiperiodic arrays of microspikes at a high number of overlapped pulses and linear polarization.[19,20] In our case, at very low scanning speed, corresponding to optimal conditions for the formation of microspikes, i.e., at a high number of overlapped shots, the meshes started to deform due to accumulating heat and destruction of wires. Because of this, we limited our experiments with 50 mm/s as the lowest scanning speed.
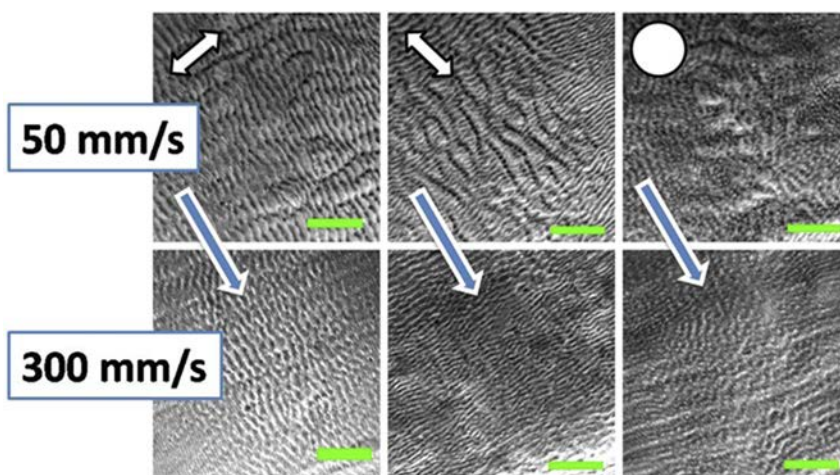

FIG. 3. SEM images of the laser-textured samples prepared in ambient air. Blue arrows show the direction of scanning by the laser beam. The direction of polarization is marked with white arrows in the case of linear polarization and with a white circle in the case of circular polarization. The green scale bar in the bottom right corner of SEM images has a length equal to 10 μm.

During these experiments, laser induced periodic surface structures (LIPSSs) in the form of ripples with a period close to the value of the laser wavelength and with the direction perpendicular to the laser polarization were formed (Fig. 3, 300 mm/s row, left and center). With the increasing number of overlapped pulses (i.e., decreasing scanning speed), the microgrooves with a period of a few laser wavelengths directed mainly parallel to the polarization direction appeared alongside the LIPSSs (Fig. 3, 50 mm/s row, left and center). In the case of circular polarization, the ripples were replaced with micropikes. With the increasing number of pulses, larger structures in the form of hills can be observed (Fig. 3, right).

The SEM images of the textured surfaces in the case of different gas environments are shown in Fig. 4. The same, as for Fig. 3, trend was observed. In general, there was no large difference in textured surfaces for different gases and vacuum. The resulting morphology was very similar for different gases, suggesting that any observed roughness variations had no relations with the gas environment. Note that in the case of SF_6, a suppression of the formation of LIPSSs due to chemical reactivity was reported.[21] We did not observe this effect probably due to lower laser fluence and a smaller number of overlapped pulses compared with the experimental conditions in Ref. 21.

B. Vacuum storing

In this subsection, we address the effect of aging in vacuum on the wettability transformation of metal surfaces textured in air. It has been reported that storing laser-treated samples in vacuum allows increasing the hydrophobic properties during a much shorter (of a few hours) period of time, compared with the time required for the same transformation through aging in air.[22,23] This behavior was attributed to the presence of hydrocarbons in the form of contaminations from the oil used for the lubrication of moving parts of vacuum pumps. We address this problem since in our experiments, the mesh samples were treated by laser radiation inside the chamber at vacuum conditions or in a gas environment under pressure (200 mbar) still lower than the atmospheric one and then stored for a period of 2 h. The goal was to clarify and separate the possible side effects from the vacuum environment.

For the above purposes, four sets of samples were prepared in atmospheric air. After laser treatment, the first set was tested for the WCA after keeping the sample for 1 h in air. This measurement served as a reference for the three other sets. The second set of samples was stored in the ambient atmosphere for 12 h at the conditions described in Sec. II. The third and fourth sets of samples were placed in Chamber No. 1 and Chamber No. 2,
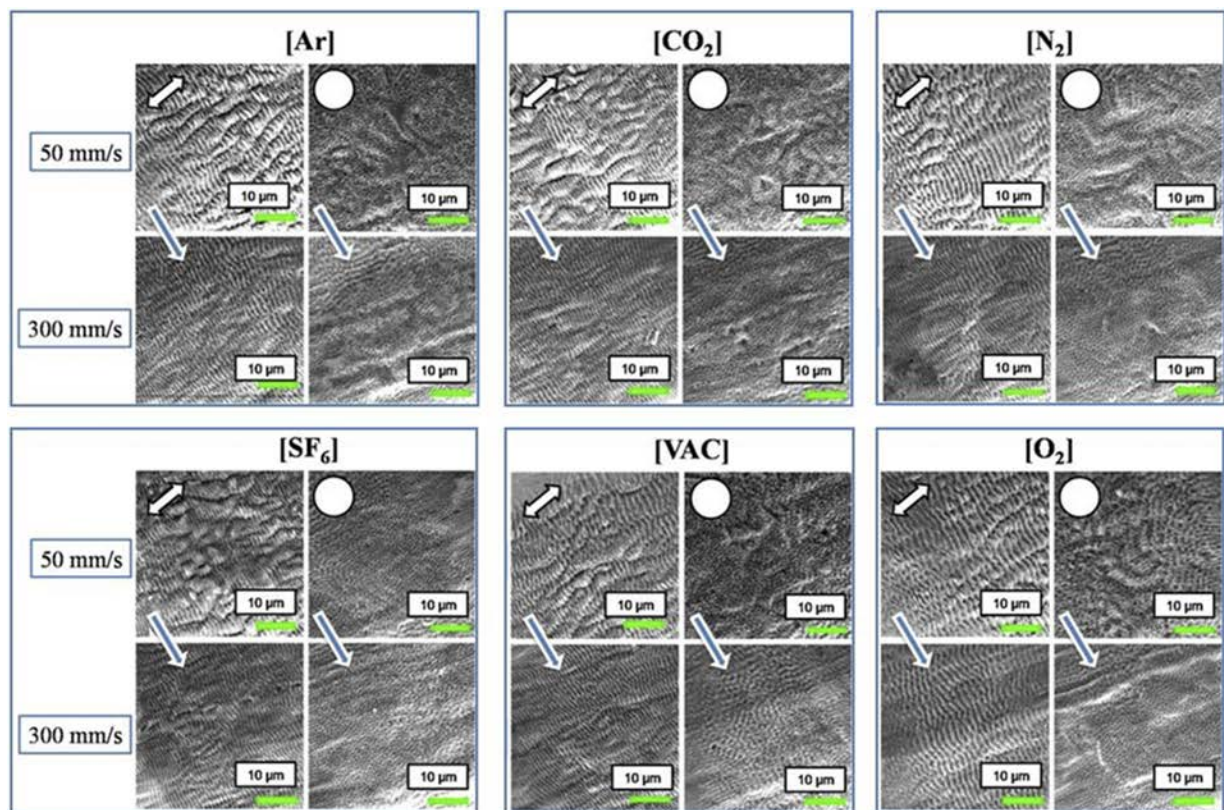

FIG. 4. SEM images of the laser textured samples prepared in various gas environments and at the vacuum conditions. Blue arrows show the direction of the scanning by the laser beam. The direction of polarization is marked with white double side arrows in the case of linear polarization and with white circles in the case of circular polarization.

respectively, for 12 h of vacuum storage. After storing for the given period of time, the WCA of one air set and two vacuum sets of samples was measured.

The results of this experiment are shown in Fig. 5. The black solid line with solid squares shows the dependence of the WCA on the scanning speed in the case of the set kept in air for 1 h after LIPSS formation. As expected, after texturing in air, the wettability of the sample became hydrophilic ($\theta_w < 90°$). The WCA increased once the scanning speed increased from 50 to 300 mm/s. The second set aged in air for 12 h (Fig. 5, red solid line with solid circles) still demonstrated the hydrophilic properties. The WCA for the low scanning speeds remained almost unchanged, while for higher speeds (250–300 mm/s), it increased compared to the one tested 1 h after laser treatment while still maintaining the WCA lower than the one for the untreated mesh surface ($\theta_w = 128°$).

Meanwhile, when we compared the third and fourth sets of samples aged in vacuum inside Chamber No. 1 and Chamber No. 2 with those stored in air, a dramatic difference is observed in the WCA. For all samples stored in Chamber No. 2 (Fig. 5, blue solid line with solid triangles), the WCA shifted to the superhydrophobic region (Fig. 5, hatched gray area corresponding to WCA > 150°), while the samples stored in Chamber No. 1 (Fig. 5, green solid line with solid triangles), though showing an increase in the WCA value, still demonstrated a smaller value of this parameter compared with the untreated surface. Some increase in wettability in the latter case can be explained by the dehydration of samples in vacuum. The brown horizontal line in Fig. 5 shows the WCA for the untreated surface of the meshes. This angle had a value of ~128° and remained the same in different gas environments and vacuum aging.

LIPSS formation on metal meshes by laser texturing is a crucial and primary requirement for altering the wetting properties of materials. The WCA measurement of the freshly laser-structured stainless steel meshes in ambient air conditions demonstrated hydrophilic behavior. The unsaturated cations and anions formed after laser ablation stabilize themselves by heterolytic dissociative adsorption of H_2O molecules from the atmosphere, giving birth to a hydroxylated layer over the metal oxide layer.[24] The hydroxylated (–OH) layer has high affinity to absorb water molecules through hydrogen bonding, which explains the hydrophilic nature of freshly laser-textured surfaces. A detailed analysis of laser-structured stainless steel plates was performed in Ref. 25. Freshly prepared samples demonstrated the increase in Fe and Cr oxides and the significant presence of O^{2-}/OH^-. A significant increase in C 1s emission after vacuum treatment reported in Ref. 25 was explained by carbonaceous contamination during vacuum aging.

Our energy-dispersive x-ray (EDX) analysis of the surface chemistry confirms the conclusions of Ref. 25. Though EDX has many limitations, it can be considered as a qualitative method of surface characterization, which was used to obtain the estimation of the chemical composition at the surface. Figure 6 shows the variation of the weight percentage (wt. %) of carbon (black bars) and oxygen (cyan bars) in the case of laser treated and untreated surfaces. A significant growth of O and a decrease in C on the freshly prepared mesh microstructures are observed (R11 and R12 bars, Fig. 6). This effect, which is related to the material removal during the ablation process, can lead to surface cleaning and the oxidation of the surface material with atmospheric oxygen. In addition, note that with the decreasing scanning speed (from 300 to 50 mm/s), the amount of oxygen slightly increases due to the growing number of the overlapped laser pulses on the target surface (compare blue bars R11 and R12). After storing in air and in Chamber No. 1 for 12 h (R21 to R32 bars), the relative content of C and O remained approximately the same, which explains the similar results for the WCA in Fig. 5. In contrast, storing inside Chamber No. 2 (R41 and R42 bars) led to a notable increase in carbon with regard to oxygen.
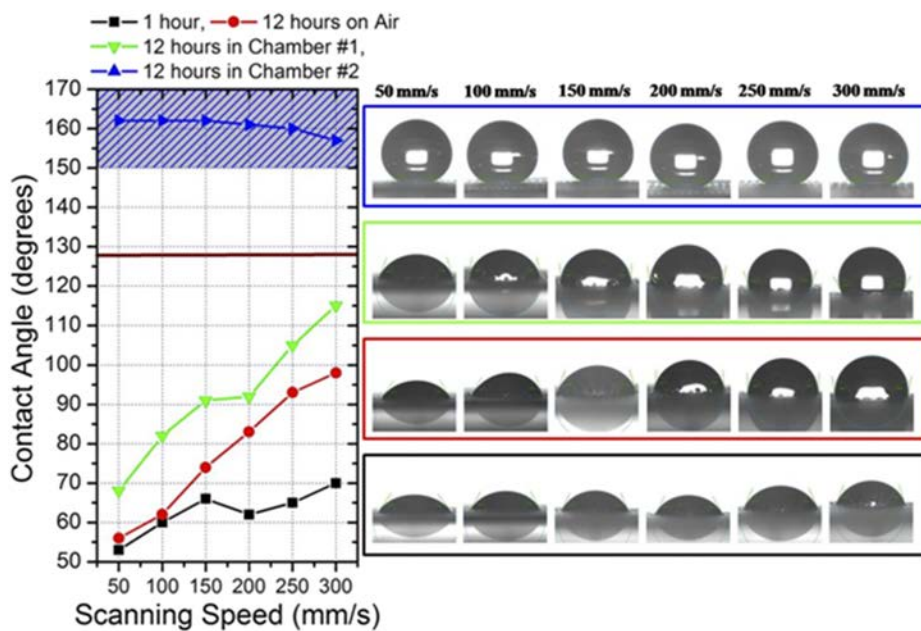

FIG. 5. Contact angle variations of the laser-treated meshes stored in air (red solid line with filled circles), vacuum Chamber No. 1 (green solid line with filled triangles), and vacuum Chamber No. 2 (blue solid line with filled triangles). Reference samples measured 1 h after laser texturing are shown by the black solid line with filled squares. On the right side, the images of the WCA recorded using a Drop Shape Analyzer are shown.
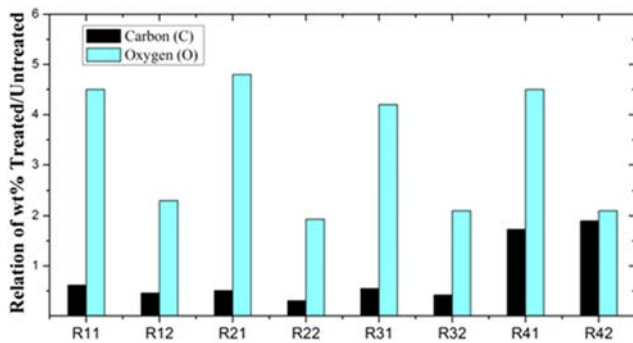
FIG. 6. EDX analysis of the relative weight variation of C (black bars) and O (cyan bars) in the case of laser-treated and untreated surfaces. Here, R11 is a ratio of elements in the case of the treated sample prepared in ambient air at a scanning speed of 50 mm/s and stored for 1 h in air after laser texturing. R12 is the same as R11 but at a scanning speed of 300 mm/s. R21 is related to the sample prepared at 50 mm/s and stored for 12 h in ambient air, and R22 is the same as R21 but at 300 mm/s. R31 is related to the sample prepared at 50 mm/s and stored for 12 h in vacuum inside Chamber No. 1, and R32 is the same as R31 but at 300 mm/s. R41 is the sample prepared at 50 mm/s and stored for 12 h in vacuum inside Chamber No. 2, and R42 is the same as R41 but at 300 mm/s.

Thus, one can conclude that vacuum conditions with hydrocarbon contamination can strongly change the surface chemistry of the laser-treated samples. The short chained non-polar hydrocarbons replaced the –OH group formed immediately after laser ablation at an accelerated rate under vacuum storage. A fast transition in the wetting state from the superhydrophilic to the superhydrophobic state is observed after vacuum aging in the contaminated chamber. For this reason, all the following SEM and EDX measurements were carried out for separately prepared samples. Further studies using different gas environments were carried out using Chamber No. 1.

C. Atmospheric air produced sample aging

Figure 7 shows the results of long-term aging of samples produced in ambient air and later stored in air at normal atmospheric pressure. In this figure, the wettability dependence on scanning speed, the morphology produced by different polarizations [designated by horizontal polarization (HP), vertical polarization (VP), and circular polarization (CP)], and the number of storage days are plotted.

The brown horizontal line depicts the WCA for the untreated surface (128°). 30 days of aging (blue solid lines) was enough for most of the samples to increase their WCA above 140°. HP-, VP-, and CP-treated samples irradiated at scanning speeds from 50 to 250 mm/s had a WCA that exceeded 145° and were close to the superhydrophobic limits, while some of them demonstrated WCA > 150°. However, the improved water contact angle for the samples processed using lower scanning speeds (50 and 150 mm/s) was observed. This increase in the WCA was attributed to the deeper and sharper surface morphology during LIPSS formation since the application of low scanning speeds results in a rougher surface, with pronounced ripples and additional structures and redeposition, while at high scanning speeds, the surface remains less deformed. The rougher surface can attract hydrocarbons presented in ambient air.

The strongly irradiated surface at initial periods of air aging demonstrates hydrophilic properties, but for later times (>2 days), the pace of changing increases and outperforms the initial WCA. The results of aging shown in Fig. 7 demonstrate no noticeable dependence on the morphology generated by applying different laser polarizations.

Figure 8 shows the relationship between the presence of C (black bars) and O (cyan bars) for mesh samples after 30 days of aging. For all samples, we see an increase in the relative amount of carbon C on the surface containing LIPSSs. This amount was lower than that in the samples stored inside Chamber No. 2 (Fig. 5), which would explain the lower WCA in the case of air aged samples.
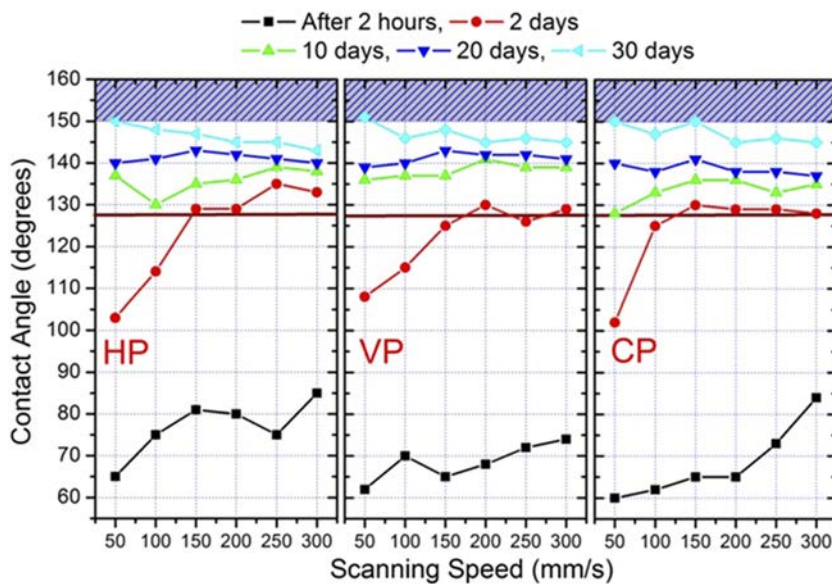

FIG. 7. Evolution of the WCA of the samples produced in ambient air and aged during 30 days in air. HP is the polarization direction of the laser field perpendicular to the direction of scanning, VP is the direction of the laser field parallel to the direction of scanning, and CP is the circularly polarized laser beam.
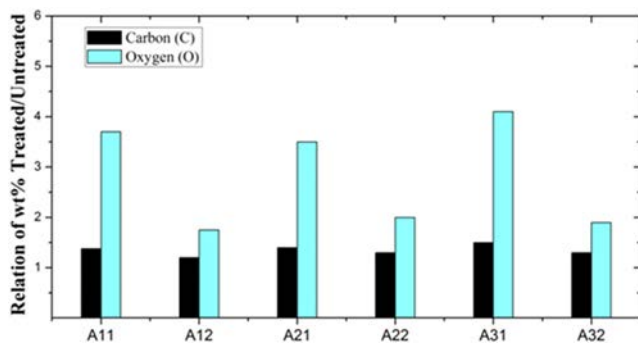
FIG. 8. EDX analysis of the variations of the weight percentage of C (black bars) and O (cyan bars) for laser-treated and untreated surfaces after aging during 30 days in atmospheric air. Here, A11 is related to the treated/untreated sample prepared in ambient air at a scanning speed of 50 mm/s, with HP polarization, and A12 is the same as A11 but at a scanning speed 300 mm/s. A21 is related to the sample prepared at 50 mm/s, with VP polarization, and A22 is the same as A21 but at a scanning speed of 300 mm/s. A31 is related to the sample prepared at a scanning speed of 50 mm/s, with CP polarization, and A32 is the same as A31 but at a scanning speed of 300 mm/s.

D. Samples prepared in gas and vacuum

The fabrication of single- and two-dimensional LIPSSs modifies different properties of the surface depending on the surrounding environment.[26,27] Here, we present the results of aging on the samples prepared with the same laser parameters as were used in the above studies but in the presence of different gas media. These studies were performed inside "oil-free" Chamber No. 1 to exclude the possible side effects caused by hydrocarbon-induced contamination. Our experiments with gases allow us to isolate and analyze the influence of three main components of atmospheric air (N_2, O_2, and CO_2) on the variations of wettability. This approach also excludes or at least dramatically decreases the influence of the water vapor inevitably presented in any atmospheric conditions.

The samples were laser textured in pure gases, stored in the same gases for 2 h to achieve relaxation after laser treatment, and then extracted from the chamber and aged in ambient air for 30 day. The results of 30 days of air aging of the samples prepared in the corresponding gaseous media are presented in Fig. 9. One can see the common property of all gases except oxygen: WCAs are mainly less than 140°, thus showing the reduced speed of transition to the hydrophobic state. Only one set of samples prepared in the O_2 environment demonstrated a similar behavior as the air prepared samples. Probably, this observation emphasizes the role of oxides as the preferable substrate for facilitating the adsorption of the hydrocarbon layer on the surface of the laser-textured sample.

The samples prepared in SF_6 showed the slowest WCA transition speed. In addition, notice that the surface of the samples prepared in SF_6, being tested in the defined spot for the WCA, changed its wetting properties after contact with the water droplet.
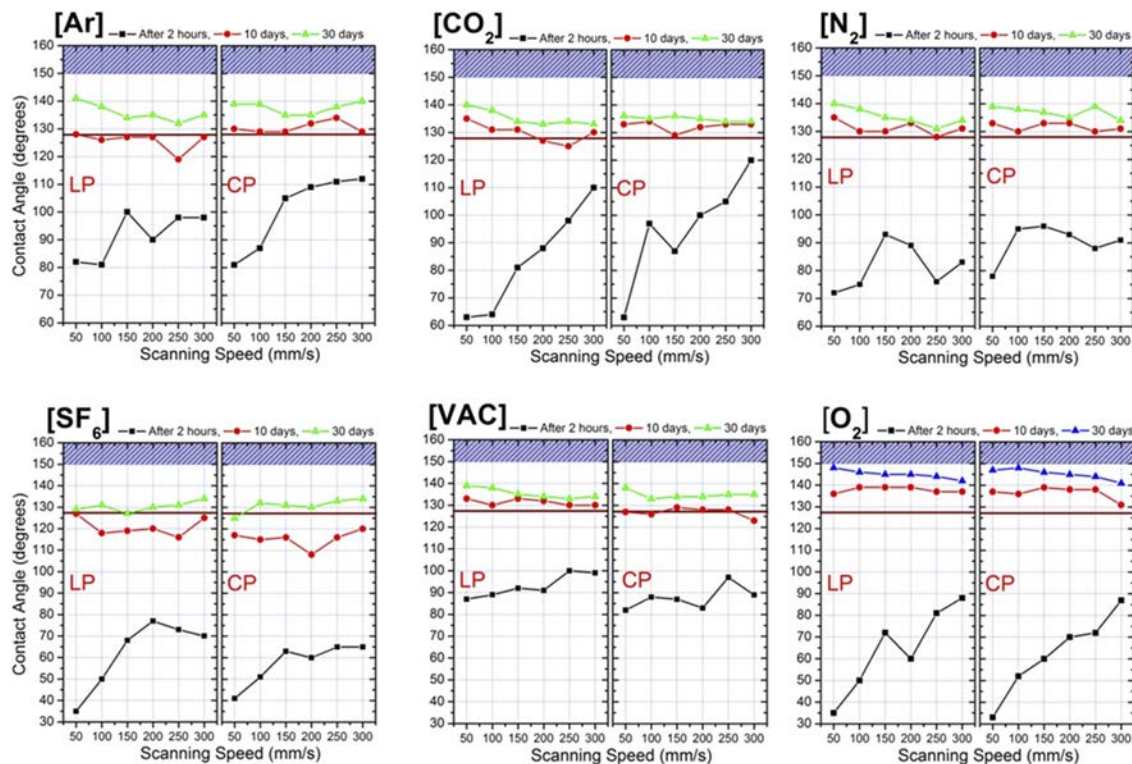

FIG. 9. Evolution of the WCA of the samples laser treated in Ar, N_2, CO_2, SF_6, vacuum, and O_2 and aged up to 30 days in ambient air. LP is the polarization direction of the laser field perpendicular to the direction of the scanning beam. CP is the circularly polarized laser beam.
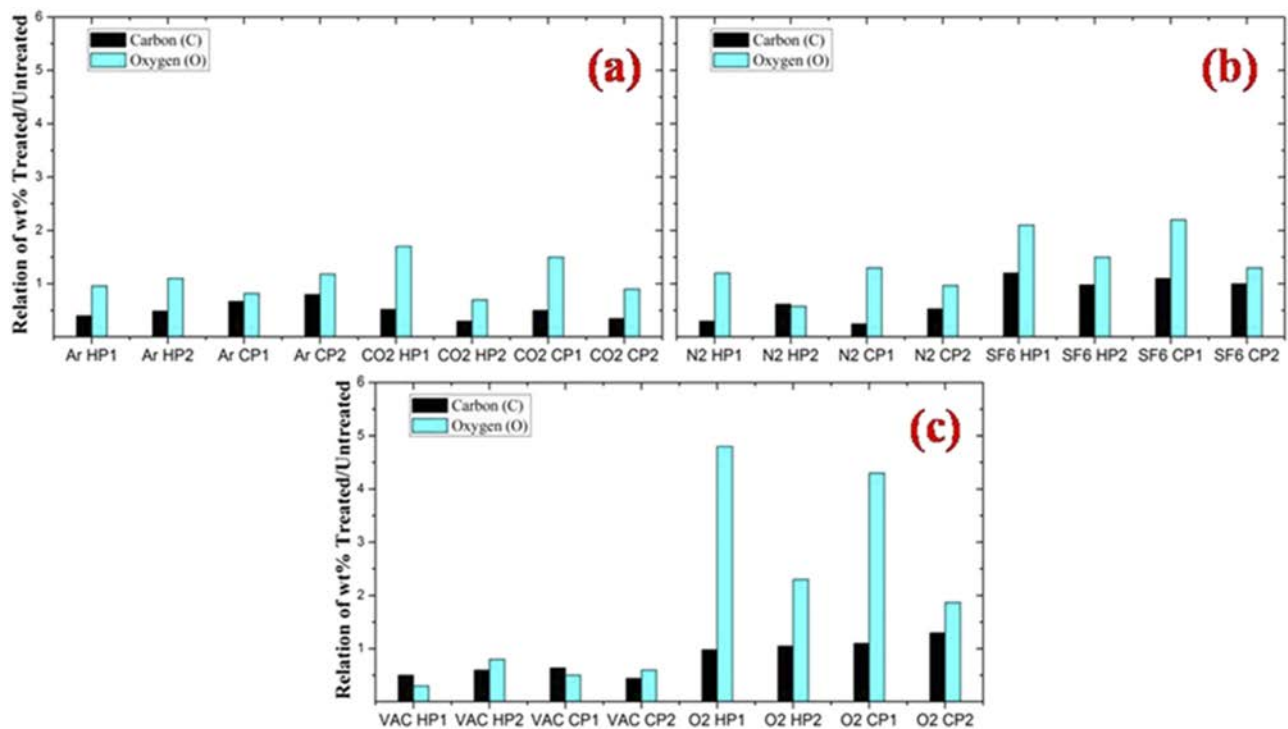
FIG. 10. EDX analysis of the change in the weight percentage (wt. %) relation between the samples treated by laser radiation in different gases and untreated surfaces for C (black bars) and O (cyan bars) elements after 30 days of aging in atmospheric air. Subscripts of bars denote the gas type: Ar and CO_2 (a), N_2 and SF_6 (b), and O_2 and VAC (vacuum conditions) (c). HP and CP correspond to horizontal and circular polarizations, similar to Fig. 7. Numbers 1 and 2 indicate the scanning speeds used (50 and 300 mm/s, respectively).

The repeated tests at the same place of these samples demonstrated a higher WCA.

Figure 10 presents the summary of the semi-quantitative analysis of the variations of weight percentage relation for laser-treated samples in different gas media and untreated surfaces after 30 days of aging in atmospheric air. The marks below the corresponding bars denote the used gases (from Ar to O_2; VAC means vacuum). HP and CP correspond to the polarization type, and the numerical values (1 and 2) correspond to the scanning speeds of 50 and 300 mm/s, respectively. In the case of O_2 [from O_2 HP1 to O_2 CP2 bars in Fig. 10(c)], a pattern similar to the one shown in Fig. 8, where stronger oxidation is accompanied by the increased presence of carbon, led to higher values of the WCA.

For SF_6 bars [from SF_6 HP1 to O_2 CP2 bars in Fig. 10(b)], we also observed the relatively high presence of carbon. Meanwhile, only in this case, among all gases, we observed the relatively high presence of one of the components of SF_6 gas, i.e., fluorine F (up to 8 wt. % in the case of the 50 mm/s scanned sample). The presence of F can lead to the formation of the metal-fluoride compounds, which may explain the unstable behavior of the samples. For other gases (Ar, N_2, and CO_2) [from Ar HP1 to CO_2 CP2 bars in Fig. 10(a) and N_2 HP1 to N_2 CP2 bars in Fig. 10(b)] and vacuum [bars VAC HP1 to VAC CP2 in Fig. 10(c)], the common features were the small additional oxidation and lesser presence of carbon, which correlate well with the measured lower values of the WCA shown in Fig. 9. We

also noticed an insignificant difference in the results produced with linear (HP) and circular (CP) polarizations when performing either the WCA or EDS measurements.

IV. CONCLUSION

Our studies have revealed the role of different gas environments during laser surface structuring followed by air aging. We have demonstrated the formation of two types of structures (ripples and spikes) when the accumulated laser fluence was varied by changing the scanning speed. We did not observe a significant dependence of the low-scale LIPSS morphology for the aged samples at the presented experimental conditions, while we observed a weak dependence on the scanning speed variations in the studied range of variations of this parameter. After 30 days of aging, the samples produced in atmospheric air and in pure O_2 have demonstrated transition toward large contact angles (WCA > 145°), while the samples prepared in Ar, CO_2, N_2, SF_6, and vacuum maintained their WCA below or at around 140°. EDX analysis has demonstrated the correlation of the amount of O and C with the observed hydrophobicity. Probably, gases, except O_2, reduce the final WCA after 30 days of aging, which was attributed to lesser oxidation, preventing the formation of a phobic layer. For stainless steel mesh, O_2 and hence oxidation play important roles in providing optimal conditions for transformation to the hydrophobic state.

AUTHORS' CONTRIBUTIONS

All authors contributed equally to this work.

DATA AVAILABILITY

The data that support the findings of this study are available from the corresponding author upon reasonable request.

REFERENCES

[1] F. Müller, C. Kunz, and S. Gräf, Materials **9**, 476 (2016).

[2] T. Nuutinen, M. Silvennoinen, K. Päiväsaari, and P. Vahimaa, Biomed. Microdevices **15**, 279 (2013).

[3] J. Long, P. Fan, D. Gong, D. Jiang, H. Zhang, L. Li, and M. Zhong, ACS Appl. Mater. Interfaces **7**, 9858 (2015).

[4] E. Skoulas, A. Manousaki, C. Fotakis, and E. Stratakis, Sci. Rep. **7**, 45114 (2017).

[5] S.-J. Park and M.-K. Seo, Interface Sci. Technol. **18**, 147 (2011).

[6] F. Chen, D. Zhang, Q. Yang, X. Wang, B. Dai, X. Li, X. Hao, Y. Ding, J. Si, and X. Hou, Langmuir **27**, 359 (2011).

[7] A. Riveiro, T. Abalde, P. Pou, R. Soto, J. del Val, R. Comesaña, A. Badaoui, M. Boutinguiza, and J. Pou, Appl. Surf. Sci. **515**, 145984 (2020).

[8] J. Long, M. Zhong, H. Zhang, and P. Fan, J. Colloid Interface Sci. **441**, 1 (2015).

[9] A.-M. Kietzig, S. G. Hatzikiriakos, and P. Englezos, Langmuir **25**, 4821 (2009).

[10] Y. Tian and L. Jiang, Nat. Mater. **12**, 291 (2013).

[11] V. D. Ta, A. Dunn, T. J. Wasley, J. Li, R. W. Kay, J. Stringer, P. J. Smith, E. Esenturk, C. Connaughton, and J. D. Shephard, Appl. Surf. Sci. **365**, 153 (2016).

[12] J. T. Cardoso, A. Garcia-Girón, J. M. Romano, D. Huerta-Murillo, R. Jagdheesh, M. Walker, S. S. Dimov, and J. L. Ocaña, RSC Adv. **7**, 39617 (2017).

[13] D. V. Ta, A. Dunn, T. J. Wasley, R. W. Kay, J. Stringer, P. J. Smith, C. Connaughton, and J. D. Shephard, Appl. Surf. Sci. **357**, 248 (2015).

[14] Z. Yang, Y. L. Tian, C. J. Yang, F. J. Wang, and X. P. Liu, Appl. Surf. Sci. **414**, 313 (2017).

[15] P. Pou, J. del Val, A. Riveiro, R. Comesaña, F. Arias-González, F. Lusquiños, M. Bountinguiza, F. Quintero, and J. Pou, Appl. Surf. Sci. **475**, 896 (2019).

[16] M. M. Gentleman and J. A. Ruud, Langmuir **26**, 1408 (2010).

[17] K. Yin, D. Chu, X. Dong, C. Wang, J.-A. Duan, and J. He, Nanoscale **9**, 14229 (2017).

[18] S. A. Khan, V. Ialyshev, V. V. Kim, M. Iqbal, H. Al Harmi, G. S. Boltaev, R. A. Ganeev, and A. S. Alnaser, Front. Chem. **8**, 768 (2020).

[19] Y. Han and S. Qu, Chem. Phys. Lett. **495**, 241 (2010).

[20] A. J. Pedraza, J. D. Fowlkes, and Y.-F. Guan, Appl. Phys. A **77**, 277 (2003).

[21] B. K. Nayak, M. C. Gupta, and K. W. Kolasinski, Appl. Phys. A **90**, 399 (2008).

[22] R. Jagdheesh and J. L. Ocaña, Mater. Lett. **270**, 127721 (2020).

[23] R. Jagdheesh, P. Hauschwitz, J. Mužík, J. Brajer, D. Rostohar, P. Jiříček, J. Kopeček, and T. Mocek, Appl. Surf. Sci. **493**, 287 (2019).

[24] A. S. Alnaser, S. A. Khan, R. A. Ganeev, and E. Stratakis, Appl. Sci. **9**, 1554 (2019).

[25] R. Jagdheesh, M. Diaz, S. Marimuthu, and J. L. Ocaña, J. Mater. Chem. A **5**, 7125 (2017).

[26] T. Jia, M. Baba, M. Suzuki, R. A. Ganeev, H. Kuroda, J. Qiu, X. Wang, R. Li, and Z. Xu, Opt. Express **16**, 1874 (2008).

[27] U. Chakravarty, R. A. Ganeev, P. A. Naik, J. A. Chakera, M. Babu, and P. D. Gupta, J. Appl. Phys. **109**, 084347 (2011).